Constrained Analysis of Fluorescence Anisotropy Decay: Application to Experimental Protein Dynamics

Efraim Feinstein,* Gintaras Deikus,[†] Elena Rusinova,[‡] Edward L. Rachofsky,* J. B. Alexander Ross,[§] and William R. Laws[§]

*Department of Pharmacology and Biological Chemistry, Mount Sinai School of Medicine, New York, New York 10029; [†]Department of Biology, City College of New York, New York, New York 10031; [‡]Department of Medicine, Mount Sinai School of Medicine, New York, New York 10029; and [§]Department of Chemistry, University of Montana, Missoula, Montana 59812

ABSTRACT   Hydrodynamic properties as well as structural dynamics of proteins can be investigated by the well-established experimental method of fluorescence anisotropy decay. Successful use of this method depends on determination of the correct kinetic model, the extent of cross-correlation between parameters in the fitting function, and differences between the timescales of the depolarizing motions and the fluorophore's fluorescence lifetime. We have tested the utility of an independently measured steady-state anisotropy value as a constraint during data analysis to reduce parameter cross correlation and to increase the timescales over which anisotropy decay parameters can be recovered accurately for two calcium-binding proteins. Mutant rat F102W parvalbumin was used as a model system because its single tryptophan residue exhibits monoexponential fluorescence intensity and anisotropy decay kinetics. Cod parvalbumin, a protein with a single tryptophan residue that exhibits multiexponential fluorescence decay kinetics, was also examined as a more complex model. Anisotropy decays were measured for both proteins as a function of solution viscosity to vary hydrodynamic parameters. The use of the steady-state anisotropy as a constraint significantly improved the precision and accuracy of recovered parameters for both proteins, particularly for viscosities at which the protein's rotational correlation time was much longer than the fluorescence lifetime. Thus, basic hydrodynamic properties of larger biomolecules can now be determined with more precision and accuracy by fluorescence anisotropy decay.

INTRODUCTION

Time-resolved fluorescence anisotropy decay is a well-established experimental method for investigating hydrodynamic properties and structural dynamics of proteins (Badea and Brand, 1979). This technique measures the time dependence of the depolarization of light emitted from a fluorophore experiencing angular (rotational) motions. For an intrinsic or extrinsic probe on a protein, these depolarizing motions include rotations of the entire macromolecule, segmental fluctuations of the domain containing the fluorophore, and local dynamics of the fluorophore about a covalent bond or within a noncovalent binding site. As a result, fluorescence anisotropy decay is useful for establishing relationships between structural dynamics and function by providing information about local motions within a specific region such as the active site of an enzyme. Time-resolved fluorescence anisotropy decay also yields overall size and shape parameters, which can provide additional information on biological function and interactions with other molecules.

To use time-resolved fluorescence anisotropy decay effectively, several factors must be considered (Rachofsky and Laws, 2000). One factor is the rate of depolarization relative to that of the fluorescence intensity decay. If the rotational correlation time (ϕ) associated with a depolarizing process is much shorter than the fluorescence lifetime (τ), the depolarization may be too rapid to be resolved. Conversely, if a depolarizing process is much slower than the decay of the excited state, little depolarization will occur before emission. A previous study has shown that the approximate range of recoverable rotational correlation times is $0.1\tau < \phi < 10\tau$ (Wahl, 1979). Because most intrinsic and extrinsic fluorophores commonly used for fluorescence anisotropy decay have lifetimes less than 5 ns, the size of spherical macromolecules or complexes that can be studied is thus restricted to molecular weights under 50 kDa. A second factor that must be considered is the possibility of multiple depolarizing motions. There may be contributions to the anisotropy decay resulting from asymmetric macromolecular rotations as well as from the segmental flexibility and other local dynamics mentioned above. More than one type of depolarizing motion, each with a characteristic rate, requires the resolution of multiple correlation times. A third factor is the possibility of multiple fluorophores in different sites but with overlapping excitation and emission contributing to the detected fluorescence. Because the local interactions and motions in each site will not be identical, different processes will depolarize each fluorophore. This situation is likely to hamper determination of the proper kinetic model that can account for all dynamic and hydrodynamic behavior of the fluorophores and the macromolecule.

The kinetic model often used to define fluorescence anisotropy decay takes the general form of a product of two exponential functions (see Materials and Methods). Consequently, there can be significant cross-correlation between

parameters recovered from data analyses, which leads to difficulties in recovery of precise and accurate anisotropy decay parameters. As outlined by Lakowicz (1999), application of global analysis methods to multiple datasets, for example those obtained as a function of excitation wavelength or quencher concentration, has been used to enhance recovery of anisotropy parameters. Recently, we presented a new approach for improving the recovery of parameters from a single time-resolved fluorescence anisotropy dataset. This procedure employs a modified Lagrange multiplier to constrain the values of iterated parameters during the analysis (Rachofsky et al., 1999). In our initial study, simulated anisotropy datasets were generated using a wide range of intensity and anisotropy decay parameters. To help assess and compare analyses, a recovery parameter was introduced based on the differences between the recovered parameters and their corresponding generation values. Those simulation studies demonstrated that application of the steady-state anisotropy as a constraint increased the accuracy of the recovered parameters. Importantly, they showed that use of the constraint significantly expanded the range of rotational correlation times that could be recovered accurately for a given fluorescence lifetime. We concluded that such a constrained analysis should greatly extend the range of macromolecular sizes that can be evaluated by time-resolved anisotropy through the use of common fluorescent probes.

We report here experimental results from application of this procedure to the time-resolved anisotropy decay of two model proteins, the cod and single tryptophan-containing mutant rat parvalbumins. These are homologous, calcium-binding proteins of the EF-hand family (Kawasaki and Kretsinger, 1994; Nakayama and Kretsinger, 1994) with very similar structures (McPhalen et al., 1994; Declerc et al., 1999; Laberge et al., 1997). The F102W mutation in the rat protein inserts a Trp residue into the same hydrophobic core region as the naturally occurring single Trp residue in the cod protein. These proteins are used as model systems because they are small and essentially spherical, with a whole-molecule rotational correlation time in a low-viscosity aqueous buffer expected to be similar to the fluorescence lifetime(s) of their Trp residue. Datasets were collected for these proteins in glycerol:aqueous buffer mixtures of varying viscosity to increase the correlation time to values much longer than the fluorescence lifetime. Comparisons between the analyses with and without the steady-state anisotropy constraint for these two model proteins demonstrate three important points. First, as suggested by the simulation studies, significantly longer correlation times can be recovered more accurately with application of the steady-state anisotropy as a constraint. Second, use of the constraint increases the *precision* of the recovered anisotropy decay parameters. Finally, application of the constraint improves the precision and accuracy of anisotropy parameters from a kinetically more complex system. Consequently, time-resolved fluorescence anisotropy decay can be used to study

larger macromolecules and complexes in solution, thereby providing useful information about basic hydrodynamic properties that helps to define their function.

MATERIALS AND METHODS

Unless specified, all chemicals were reagent grade, and all experiments were performed at 20°C.

Sample preparation

Rat parvalbumin with the F102W mutation and cod parvalbumin were generous gifts from Dr. Arthur Szabo and Dr. Lina Kalinichenko, respectively. Purification protocols have been previously described for both the rat (Pauls et al., 1993) and cod (Permiakov et al., 1987) proteins. The rat protein was prepared for use by FPLC gel filtration on a Superdex 75 HR 10/30 column (Pharmacia Biotech, Piscataway, NJ), using a 10 mM HEPES buffer, pH 7.5, containing 0.2 M NaCl and 5 mM CaCl$_2$. Experiments on both proteins were performed in a 10 mM HEPES buffer containing 0.14 M NaCl and 5 mM CaCl$_2$; the final pH of all samples was 7.5. The concentration of rat F102W parvalbumin was determined by absorbance at 280 nm, using an extinction coefficient of 5500 M^{-1}cm^{-1}, which is appropriate for one Trp and no Tyr residues (Wetlaufer, 1962). Cod parvalbumin concentration also was determined by absorbance at 280 nm, using an extinction coefficient of 7189 M^{-1}cm^{-1} (Closset, 1976), which is representative for one Trp and two Tyr residues. For both proteins, fluorescence measurements were made on ~10 μM samples.

Stock solutions of glycerol (spectroscopic grade, Mallinckrodt, Paris, KY) were prepared by mixing known weights of glycerol and buffer. Known weights (volumes) of stock protein and glycerol solutions were then mixed to generate protein solutions of different viscosity. Solution viscosities were calculated based on linear interpolations of a glycerol weight percent table (Sheely, 1932).

Spectroscopy

Absorption spectra were measured on a Hitachi U-3210 spectrophotometer, and fluorescence spectra were obtained on an SLM-4800 fluorometer converted by us into a single-photon counting instrument.

Time-resolved fluorescence decay curves were collected using time-correlated single-photon counting. Briefly, thermostatted samples in an automated sample chamber (FLASC1000 from Quantum Northwest, Spokane, WA) were excited at 4.8 MHz with ~2 ps wide pulses (full-width-at-half-maximum) of the wavelength (290 or 295 nm) and vertical polarization generated by a laser system (Verdi V10, Mira 900, and pulse picker 9200 from Coherent, Santa Clara, CA; harmonic generator 5-050 from Inrad, Northvale, NJ). Emitted photons were first selected by an emission polarizer for the desired polarization (see below), and then selected for the desired energy by a monochromator (SpectraPro-150 from Acton Research, Acton, MA) before being detected by a photomultiplier tube module (TBX-04 from IBH, Glasgow, UK) containing a preamplifier and a constant fraction discriminator. Electronics (time-to-amplitude converter 566 and multichannel buffer 921E from EG&G Ortec, Oak Ridge, TN) processed the time between an excitation and emission event to collect a decay probability histogram over 2048 channels at 24 ps/channel. Instrument response functions (light scatter) and decay curves were collected to 100,000 and 40,000 counts in the peak channel, respectively. Decays were also collected from glycerol blank solutions for the same time as the sample, and were then subtracted from sample decays before analysis.

Anisotropy decay data analysis

Fluorescence intensity decays, $I_M(t)$, were obtained under magic angle conditions (Badea and Brand, 1979) to be free of depolarization effects, and were defined as sums of exponentials:

$$I_M(t) = \frac{1}{3} \sum_{i=1}^{n} \alpha_i e^{-t/\tau_i}. \tag{1}$$

In these studies, we assume that each exponential component arises from an independent emitting state, and that excited-state reactions or interactions do not occur. This assumption is consistent with the rotamer model of Trp fluorescence in proteins (Szabo and Rayner, 1980; Petrich et al., 1983; Haydock et al., 1990; Ross et al., 1992; Willis and Szabo, 1992; Kim et al., 1993), in which the rotamers interconvert much slower than the decay of the excited state. Accordingly, each τ_i term represents the lifetime of an individual emitting species (rotamer), and the preexponential α_i values are weighting terms that depend on several factors including concentrations, extinction coefficients, and spectral selection of the species, as well as instrumental parameters.

The anisotropy decay, $r(t)$, is related to the decays collected at emission polarizer angles of $0°$ and $90°$, or vertical and horizontal, which are represented by $I_V(t)$ and $I_H(t)$, respectively, according to:

$$I_V(t) = I_M(t)\{1 + 2r(t)\} \tag{2}$$

$$I_H(t) = I_M(t)\{1 - r(t)\}. \tag{3}$$

The anisotropy decay of a sample consists of the anisotropy decay of each emitting species, $r_i(t)$. As defined in Eq. 4, each $r_i(t)$ can be a sum of exponentials, where the preexponential terms β_{ij} denote the extent to which each emitting species is depolarized by the various motions, and the ϕ_j represent all the rotational correlation times resulting from the depolarizing motions:

$$r_i(t) = \sum_{j=1}^{m} \beta_{ij} e^{-t/\phi_j}. \tag{4}$$

The sum of the β_{ij} values over all depolarizing motions for each emitting species provides the limiting anisotropy, r_{0i}, for that species.

In general, the total anisotropy decay is:

$$r(t) = \frac{\sum_{i=1}^{n} \left\{ \alpha_i e^{-t/\tau_i} \sum_{j=1}^{m} \beta_{ij} e^{-t/\phi_j} \right\}}{\sum_{i=1}^{n} \alpha_i e^{-t/\tau_i}}. \tag{5}$$

Whereas it is generally assumed that each fluorophore is subject to all of the depolarizing motions, use of Eq. 5 permits unique lifetime-correlation time associations through β_{ij} values. For example, if a β_{ij} term equals zero, then the fluorophore whose decay results in lifetime τ_i is not depolarized by the motion leading to correlation time ϕ_j. Details concerning this description of fluorescence anisotropy decay have been published previously (Bialik et al., 1998; Rachofsky and Laws, 2000).

The $I_M(t)$, $I_V(t)$, and $I_H(t)$ decay curves for a sample, which constitute an anisotropy dataset, were analyzed simultaneously (globally) to recover the intensity and anisotropy decay parameters (Waxman et al., 1993). This analysis procedure fits the collected decay curves directly, instead of fitting sum and difference curves generated from the primary data, or even the constructed $r(t)$ decay itself. Manipulation of the primary data can result in problems with parameter recovery and error propagation (Cross and Fleming, 1984). By analyzing the primary curves simultaneously, the intensity decay parameters are common to all three decay curves, and the anisotropy decay parameters are common to two decay curves. Consequently, as with any global analysis, the number of iterated parameters is decreased, and the common parameters are over-determined. Decays were analyzed by a reconvolution procedure (Grinvald and Steinberg, 1974) using nonlinear least squares regression (Bevington, 1969). Global analyses (Knutson et al., 1983; Beechem et al., 1983) were also performed on anisotropy datasets collected as a function of viscosity. Joint support plane confidence intervals were calculated for all iterated parameters by the approximation method described by Johnson and coworkers (Straume et al., 1991).

Data analysis constrained by the steady-state anisotropy

The analysis approach that we previously introduced to improve the accuracy and precision of iterated anisotropy decay parameters (Rachofsky et al., 1999) has the same objective of all nonlinear least squares fitting algorithms: to minimize the reduced χ^2, the weighted sum of the squared residuals for each data point (Bevington, 1969). This method, however, defines a new minimization function, χ_C^2, by addition of a constraint term:

$$\chi_C^2 = \chi^2 + \kappa g, \tag{6}$$

where g is a function defining the constraint, and κ is a weighting factor theoretically equal to the inverse of the variance (square of the standard deviation), or experimental uncertainty, in this function (Rachofsky and Laws, 2000).

To constrain by the measured steady-state anisotropy, r_{ss}, the constraint function is defined as:

$$g = (r_{ss} - r_{calc})^2, \tag{7}$$

with r_{calc} representing the value of the steady-state anisotropy calculated from the iterated intensity and anisotropy decay parameters for each successful iteration. For a simple system with just one lifetime and one rotational correlation time ($n = m = 1$), r_{calc} is:

$$r_{calc} = r_0/(1 + \tau/\phi). \tag{8}$$

For a more complex kinetic system, r_{calc} may be determined by integration of Eq. 5 with respect to time as previously reported (Bialik et al., 1998).

Our previous study demonstrated that κ could differ from the inverse of the variance by several orders of magnitude, consistent with a standard deviation in r_{ss} greater than 0.001 and less than 0.0001, and still be effective with no significant change in analysis results (Rachofsky et al., 1999). For the constrained analyses presented here, κ was an empirically determined constant of 10^8.

To determine r_{ss}, four blank-corrected intensities, I_{VV}, I_{VH}, I_{HH}, and I_{HV}, were measured, where the first and second subscripts represent the vertical or horizontal polarization of the excitation beam and the orientation of the emission polarizer, respectively. To obtain I_{HH} and I_{HV} with a laser system that provides vertically polarized light, a half-wave plate located in the excitation optical pathway was used to rotate the laser beam polarization by $90°$, and a horizontally oriented polarizer was then employed to filter out any residual vertically polarized light. By definition (Lakowicz, 1999), r_{ss} is:

$$r_{ss} = (I_{VV} - GI_{VH})/(I_{VV} + 2GI_{VH}), \tag{9}$$

where G is I_{HV}/I_{HH} and corrects for unequal instrumental response to the different planes of polarization of emitted light monitored. Steady-state anisotropy values were obtained, under the same instrumental conditions, with the fluorometer used to collect decay curves to account for the narrow bandwidth (<1 nm) of the exciting laser beam and the complex excitation wavelength dependence of the tryptophan principal polarization spectrum.

Analysis acceptance criteria

Several criteria were employed to evaluate the quality of an analysis and thus allow acceptance of the recovered parameters. All fits were judged by the reduced χ^2 (or χ_C^2), weighted residuals, and autocorrelation of the residuals. Recovered lifetimes had to be consistent with those recovered from other datasets. The results of an analysis were also judged to be acceptable provided the recovered anisotropy parameters were physically relevant (β terms between 0 and 0.4 and ϕ values less than 500 ns).

In addition to these standard tests of analysis quality, another specific criterion was introduced: an analysis was judged as acceptable if the recovered correlation time agreed with the expected value to within the

experimental uncertainty in those values. The expected values of correlation times as a function of viscosity were computed according to the Stokes-Einstein equation as expected based on the structure of rat and other parvalbumins (McPhalen et al., 1994; Kretsinger and Nockolds, 1973; Kretsinger, 1980). The Stokes-Einstein relationship is $\phi = \eta V/RT$, where η is the solution viscosity, V is the molecular volume assuming a hydration of 0.27 mL/g, R is the gas constant, and T is the temperature of the solution (Lakowicz, 1999). The correlation times recovered from analyses of datasets obtained for 1 cP samples were used as the reference values ($\phi_{\eta=1}$) for the calculation of expected correlation times at higher viscosities ($\phi_{\eta>1} = \eta\phi_{\eta=1}$). The uncertainty region was defined as the rectangular area in correlation time versus viscosity space bordered by the recovered correlation time's 95% confidence limits and the uncertainty in the sample's viscosity. The 95% confidence interval is analogous to a two-standard deviation error interval in a symmetric system (Straume et al., 1991). The error in glycerol concentration, arising from weighing and pipeting errors, was estimated to be 1% (wt/wt) and accounts for any secondary effect on viscosity due to the presence of salt. This error is particularly a concern at higher glycerol concentrations, where a small change drastically affects viscosity. The viscosities calculated from those 1% concentration differences therefore defined the asymmetric error interval in viscosity. This two-dimensional uncertainty region in the recovered correlation time was compared to the expected value at each viscosity.

RESULTS

Rat parvalbumin anisotropy decays: single lifetime, single correlation time

To test the ability of an analysis constrained by the steady-state anisotropy to recover correlation times significantly longer than the fluorescence lifetime, we searched for an experimental system in which the molecular rotation rate of a spherical protein could be varied in a predictable manner by the addition of glycerol to increase solution viscosity. We used four selection criteria to keep the system as simple as possible. First, the probe should be buried in the hydrophobic core of the protein so that altering the solvent composition will minimally perturb its spectroscopic properties. Second, the fluorophore should exhibit monoexponential intensity decay with a lifetime independent of glycerol concentration. Third, the probe should be rigidly held in place so that rotation of the protein is the only depolarizing motion. Fourth, the protein should be essentially spherical, and therefore exhibit a single correlation time.

Based on these criteria, we identified the calcium-bound form of rat F102W parvalbumin, an 11.8 kDa protein, as a potential experimental model. It has previously been shown that the fluorescence intensity decay of the single Trp residue in this form of the protein is monoexponential with a lifetime near 4 ns (Pauls et al., 1993). Using the Stokes-Einstein relationship, we calculated that this protein should have a rotational correlation time of ~5 ns at 20°C; this estimated time was substantiated by a Perrin plot ($1/r_{ss}$ versus T/η, not shown). Preliminary time-resolved fluorescence experiments confirmed that the intensity decay is single exponential, but more importantly demonstrated a single rotational correlation time near 5.5 ns for the protein in aqueous buffer at 20°C. As shown in Fig. 1, rat F102W
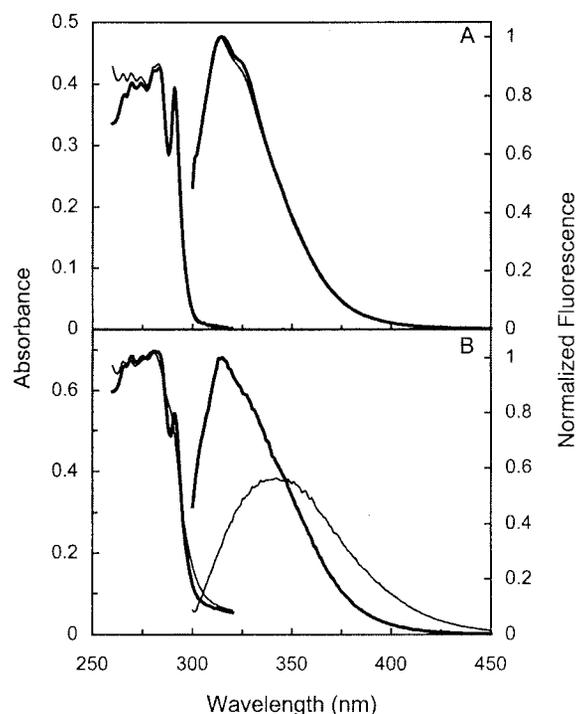
FIGURE 1 Absorbance and corrected fluorescence emission spectra for ~10 μM rat F102W (*panel A*) and cod parvalbumin (*panel B*). Thin line: apo form of protein. Thick line: calcium-bound form. The emission spectra were obtained using 295-nm excitation, and 4-nm bandpasses were used on both the excitation and emission monochromators. In panel *A*, the emission spectra are normalized to equivalent quantum yields. In panel *B*, the emission spectra are from samples with equal protein concentrations under the same instrumental conditions, and depict the differences in quantum yield and spectral position between the apo and Ca^{2+}-bound forms of the cod parvalbumin.

parvalbumin also has the other features required for the model system. The red-shifted absorption spectrum with well-resolved vibronic structure and blue-shifted emission spectrum together confirm that W102 is buried within the hydrophobic core of the protein. Moreover, addition of glycerol did not perturb these spectra (not shown). Fig. 1 also demonstrates that the presence or absence of Ca^{2+} does not affect the absorption and emission spectra (see Discussion). The calcium-bound form was chosen for the viscosity dependent experiments described below because it is easier to maintain the fully liganded state.

A series of anisotropy datasets were collected for the rat F102W parvalbumin as a function of viscosity. For these datasets, excitation was at 295 nm and the emission monochromator was set to 320 nm with a 10-nm bandpass. Analyses of the datasets were performed both with and without the steady-state anisotropy constraint. As shown by the χ^2 terms listed in Table 1, or by weighted residuals and autocorrelation of residuals (not shown), equally excellent fits were obtained with or without the constraint. In general, χ^2 terms did increase slightly on application of the r_{ss} constraint, as expected for any fitting routine when the

TABLE 1 Effect of r_{ss} constraint on recovery of rat F102W parvalbumin anisotropy decay parameters with 295-nm excitation

					Without constraint			With constraint			
η^*	ϕ_e (ns)[†]	ϕ_e/τ[§]	n[¶]	τ (ns)[‖]	ϕ (ns)[**]	r_0[††]	χ^{2}[§§]	ϕ (ns)[**]	r_0[††]	χ_C^{2}[§§]	r_{ss}[¶¶]
1.0	5.7	1.4	2	4.10 (4.10–4.11)[‖‖]	5.4 (5.2–5.5)	0.202 (0.199–0.205)	1.082	5.7 (5.6–5.8)	0.207 (0.206–0.209)	1.087	0.119
1.9	10.8	2.6	2	4.08 (4.07–4.09)	9.9 (9.4–10.6)	0.201 (0.195–0.208)	1.031	10.2 (9.9–10.4)	0.204 (0.202–0.205)	1.032	0.144
4.0	22.8	5.6	2	4.07 (4.06–4.07)	18.5 (17.1–20.3)	0.164 (0.154–0.176)	1.071	24.7 (23.6–25.7)	0.214 (0.211–0.216)	1.073	0.180
5.8	33.1	8.3	1	4.01 (4.00–4.01)	25.9 (21.6–30.3)	0.149 (0.126–0.174)	1.124	36.1 (34.9–37.4)	0.206 (0.205–0.207)	1.131	0.183
7.8	44.5	11.3	1	3.95 (3.94–3.96)	31.9 (29.3–35.8)	0.135 (0.131–0.139)	1.103	45.6 (42.7–48.7)	0.206 (0.204–0.209)	1.098	0.185
16.3	93	23.7	3	3.92 (3.91–3.93)	42.3 (36.3–50.2)	0.087 (0.079–0.095)	1.076	80.8 (72.9–89.5)	0.207 (0.207–0.210)	1.081	0.192
33.9	193	49.9	1	3.87 (3.86–3.88)	67 (47–115)	0.046 (0.045–0.048)	1.061	139 (116–167)	0.209 (0.207–0.212)	1.071	0.198
68.7	392	103	1	3.80 (3.79–3.80)	122 (80–228)	0.075 (0.064–0.086)	1.098	148 (131–169)	0.216 (0.216–0.218)	1.102	0.201

*Viscosity (in cP).

[†]The expected ϕ based on the ϕ recovered at 1 cP and the linear relationship between ϕ and η (Stokes-Einstein equation; see text).

[§]Ratio of expected correlation time to measured lifetime.

[¶]Number of datasets. If $n > 1$, the reported results are averages except for χ^2.

[‖]Recovered fluorescence intensity decay lifetime.

[**]Recovered rotational correlation time.

[††]Recovered limiting anisotropy.

[§§]The reduced, weighted sum of residuals. If $n > 1$, the reported value is for one representative dataset.

[¶¶]The measured steady-state anisotropy used as the constraint.

[‖‖]95% confidence interval.

possible range of values for one or more iterated parameters is restricted. An occasional small decrease in χ^2 was recovered, of the same magnitude of the increases generally observed, as demonstrated by the 7.8 cP results in Table 1.

Recovered correlation times are shown in Fig. 2 and Table 1. To assess the effectiveness of the constraint, it was necessary to establish guidelines for the expected precision and accuracy of a recovered correlation time. A recovered correlation time was defined as acceptable if the range of expected values intersected the rectangular area delineating the uncertainty in the value (see Materials and Methods). Because the correlation time recovered at 1 cP had a 2% uncertainty (Table 1), all calculated correlation times were assumed to inherit this 2% uncertainty. The shaded area in Fig. 2 represents this range of expected correlation times. The rectangular uncertainty region in Fig. 2 is defined by the error bars that represent the 95% confidence interval in the recovered correlation time and the estimated 1% error in glycerol concentration. Without the constraint, the recovered correlation times are acceptable for a viscosity up to 2 cP (ϕ/τ ratio ~3). Above this viscosity, the recovered values are smaller than the predicted values. With the constraint, however, the recovered and expected correlation times agree for viscosities up to 16 cP, which is a ϕ/τ ratio above twenty (Fig. 2, Table 1).

Provided the local environment of the Trp residue does not change upon addition of glycerol, the limiting anisotropy, r_0, should be constant with viscosity. This criterion also can be used to compare constrained and unconstrained analyses. Because rat F102W parvalbumin has a single correlation time, the preexponential factor β (Eq. 4) will be equal to r_0. Without the r_{ss} constraint, only the r_0 value recovered for the 2 cP dataset is within 10% of the value at 1 cP (Table 1). Above that viscosity, the recovered r_0 decreases significantly. With the constraint, however, the r_0 values are
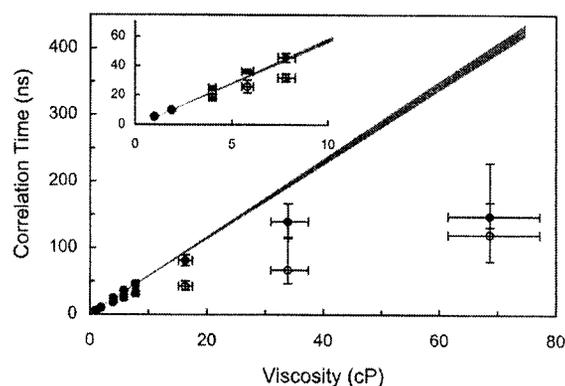
FIGURE 2 Correlation times (ϕ) versus solution viscosity for rat F102W parvalbumin excited at 295 nm. The shaded area represents a 2% interval about the expected rotational correlation times (ϕ_e, see text and Table 1). Circles represent maximum likelihood values, with filled/open for analyses with/without the r_{ss} constraint. X axis error bars represent uncertainty in viscosity for a given sample, whereas y axis error bars represent the 95% confidence interval in the recovered value. Inset: enlargement of low viscosity region.

within 5% of one another for all viscosities examined (Table 1). It should be noted that an r_0 value near 0.2 is in the range expected for 295-nm excitation of a Trp residue in a hydrophobic environment (Eftink et al., 1990).

Our initial simulation studies assessing the effectiveness of the r_{ss} constraint indicated that the ability to recover accurate anisotropy decay parameters decreases with smaller r_0 values (Rachofsky et al., 1999). This prediction can be easily tested with rat F102W parvalbumin because, as demonstrated in the principal polarization spectrum (r_0 versus excitation wavelength) of tryptophan, r_0 decreases dramatically between 295 and 290 nm (Eftink et al., 1990). Consequently, another series of rat F102W parvalbumin anisotropy datasets were collected with an excitation wavelength of 290 nm. All other experimental parameters remained the same, and the datasets were analyzed in a similar manner resulting in excellent, equivalent fits with or without the constraint as indicated by the χ^2 terms in Table 2. The recovered correlation times and their uncertainty region were compared with the expected range of values (shaded area in Fig. 3) based on the 8% uncertainty in the value of ϕ at 1 cP (Table 2). As shown in Fig. 3 and Table 2, the recovery of r_0 terms and longer correlation times from datasets obtained with 290-nm excitation is improved with the constraint. However, with or without the constraint, recovery of acceptable correlation times is over a smaller range of viscosities (lower ϕ/τ ratios) than observed with 295-nm excitation. In addition, it should be noted that

analyses of datasets collected with 290-nm excitation were more sensitive to the initial values (guesses) of the iterated parameters, and at the highest viscosities the constraint was required to recover physically relevant parameters.

Several points should be made about the recovered fluorescence lifetimes presented in Tables 1 and 2. A small but significant decrease in the fluorescence lifetime was observed with increasing glycerol concentration (from 4.1 to 3.8 ns for 1–69 cP, respectively), even though there are no significant spectral changes (see above). However, as expected for a single Trp residue in one conformation, the same lifetime was obtained at each glycerol concentration with excitation at either 290 or 295 nm. In agreement with our previous studies (Rachofsky et al., 1999), the r_{ss} constraint did not affect intensity decay parameters, as recovered lifetimes were the same with or without the constraint (not shown). Analyses of the intensity decay from the $I_M(t)$ curves alone yielded identical results.

We have also examined percent uncertainties in the recovered parameters as another way to assess the ability of the steady-state anisotropy constraint to help recover anisotropy parameters. A parameter's percent uncertainty is defined as 100 times the magnitude of its 95% confidence interval divided by its maximum likelihood value. Percent uncertainties were calculated based on the data in Tables 1 and 2. As presented in Fig. 4 A, the effect of the r_{ss} constraint is dramatic on the percent uncertainty in correlation times. For the correlation times recovered from the datasets

TABLE 2 Effect of r_{ss} constraint on recovery of rat F102W parvalbumin anisotropy decay parameters with 290-nm excitation

					Without constraint			With constraint			
η^*	ϕ_e (ns)[†]	ϕ_e/τ[§]	n[¶]	τ (ns)[‖]	ϕ (ns)**	r_0[††]	χ^{2}[§§]	ϕ (ns)**	r_0[††]	χ^{2}_C[§§]	r_{ss}[¶¶]
1.0	5.7	1.4	3	4.14 (4.14–4.15)[‖‖]	4.7 (4.0–5.5)	0.045 (0.042–0.048)	1.077	5.7 (5.3–6.2)	0.047 (0.045–0.048)	1.078	0.0267
1.9	10.8	2.7	2	4.05 (4.04–4.06)	8.0 (6.5–10.0)	0.045 (0.040–0.050)	1.031	10.2 (9.5–11.1)	0.050 (0.048–0.051)	1.038	0.0266
3.8	21.7	5.5	3	3.93 (3.92–3.95)	13.5 (9.5–19.4)	0.034 (0.028–0.042)	1.042	22.3 (19.1–25.9)	0.051 (0.049–0.052)	1.044	0.0353
5.8	33.1	8.6	1	3.84 (3.84–3.85)	5.8 (4.3–8.0)	0.016 (0.014–0.019)	1.104	35.9 (29.7–41.6)	0.050 (0.049–0.051)	1.073	0.0420
7.8	44.5	11.6	2	3.83 (3.82–3.84)	10.5 (7.9–14.3)	0.020 (0.017–0.022)	1.087	34.9 (28.4–42.9)	0.051 (0.049–0.052)	1.089	0.0442
16.3	93	24.8	1	3.75 (3.74–3.76)	***	***	***	48 (37–63)	0.048 (0.047–0.049)	1.105	0.0437
33.9	193	52.6	2	3.67 (3.67–3.68)	***	***	***	69 (50–96)	0.052 (0.051–0.053)	1.087	0.0485

*Viscosity (in cP).

[†]The expected ϕ based on the recoverd ϕ at 1 cP and the linear relationship between ϕ and η (Stokes-Einstein equation; see text).

[§]Ratio of expected correlation time to measured lifetime.

[¶]Number of datasets. If $n > 1$, the reported results are averages except for χ^2.

[‖]Recovered fluorescence intensity decay lifetime.

**Recovered rotational correlation time.

[††]Recovered limiting anisotropy.

[§§]The reduced, weighted sum of residuals. If $n > 1$, the reported value is for one representative dataset.

[¶¶]The measured steady-state anisotropy used as the constraint.

[‖‖]95% confidence interval.

***Dataset could not be analyzed for relevant anisotropy decay parameters without the constraint.
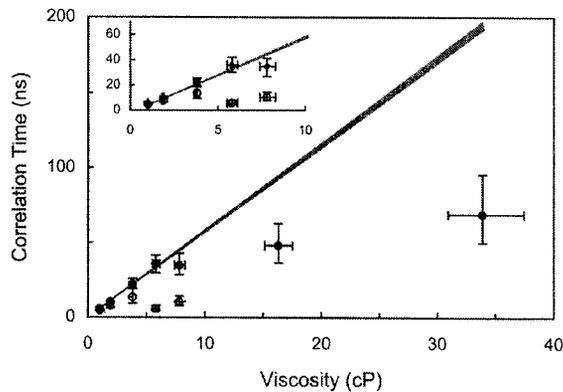
FIGURE 3 Correlation times (ϕ) versus solution viscosity for rat F102W parvalbumin excited at 290 nm. The shaded area represents an 8% interval about the expected rotational correlation times (ϕ_e, see text and Table 2). Circles represent maximum likelihood values, with filled/open for analyses with/without the r_{ss} constraint. X axis error bars represent uncertainty in viscosity for a given sample, whereas y axis error bars represent the 95% confidence interval in the recovered value. Inset: enlargement of low viscosity region.

FIGURE 4 Percent uncertainties in iterated parameter values as a function of viscosity for rat parvalbumin. (A) Uncertainties in recovered correlation times. (B) Uncertainties in recovered β terms. Squares and solid lines: from analyses of datasets collected with 295-nm excitation. Triangles and dashed lines: from analyses of datasets collected with 290-nm excitation. Filled/open markers represent analyses with/without the r_{ss} constraint. Lines connect related data points and do not represent any model.

collected at both excitation wavelengths, the percent uncertainty is always less with use of the constraint. Although the percent uncertainties in ϕ increase at higher viscosities in both constrained and unconstrained analyses, the rate of increase is much smaller when the constraint is applied. The effect of the constraint is also apparent for the percent uncertainties in the recovered β terms (Fig. 4 B). The percent uncertainty in the β parameter remains nearly constant and small in the constrained analyses of datasets collected at both excitation wavelengths. In contrast, there is no pattern in the larger percent uncertainties for the β parameters obtained from unconstrained analyses. Fig. 4 further demonstrates that a small r_0 value adversely affects parameter recovery. As expected, the percent uncertainties for both β and ϕ from the analyses of 295-nm datasets were smaller than those from 290-nm datasets.

Cod parvalbumin anisotropy decays: multiple lifetimes, single correlation time

Most single Trp-containing proteins exhibit multiexponential intensity decay kinetics. To assess the ability of the constrained analysis method to process anisotropy decay curves exhibiting multiexponential kinetics, we used the Ca^{2+}-bound form of cod parvalbumin. This protein also contains a single Trp residue, but differs from the rat mutant parvalbumin in that the fluorescence intensity decay is not monoexponential (Eftink and Wasylewski, 1989; Hutnik et al., 1990). Although the structure of cod parvalbumin has not been solved, the structures of homologous EF-hand parvalbumins (Declerc et al., 1999) and the calculated structure for cod parvalbumin (Laberge et al., 1997) suggest
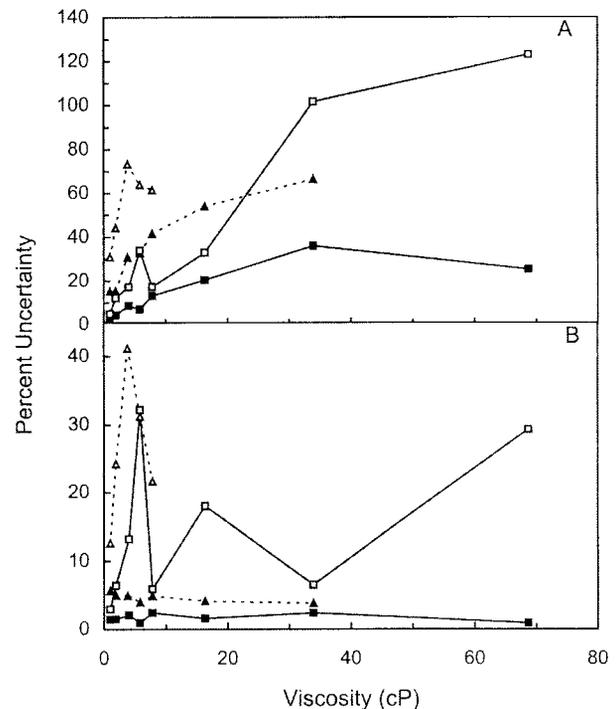
that the cod Trp residue resides in a hydrophobic core similar to that of the single Trp in the rat F102W parvalbumin. As shown in Fig. 1 B, this is supported by the absorbance and emission spectra of the Ca^{2+}-bound form of the cod protein, which are quite similar to those of the rat protein. As was found with the rat protein, the spectra for the Ca^{2+}-bound cod parvalbumin do not change on addition of glycerol (not shown). However, in contrast to the rat protein, and as previously observed (Permiakov et al. 1987; Eftink and Wasylewski, 1989; Hutnik et al., 1990), cod parvalbumin exhibits a distinctive spectral change and a corresponding loss ($\sim$1.6-fold) of quantum yield when it changes from the Ca^{2+}-bound to the apo form (Fig. 1 B).

Fluorescence anisotropy datasets as a function of viscosity were obtained for cod parvalbumin using 295-nm excitation; the same instrumental conditions were employed as in the rat protein studies except that emission was monitored at 340 nm. As shown in Table 3, the intensity decay of the cod protein is more complex kinetically than that of the rat protein: a sum of two exponential components is required to fit the data for all viscosities. Similar intensity decay results for the emission from the single Trp residue in cod parvalbumin have been reported previously (Eftink and Wasylewski, 1989; Hutnik et al., 1990). The two exponential

TABLE 3 Effect of r_{ss} constraint on recovery of cod parvalbumin anisotropy decay parameters with 295-nm excitation

η^*	$n^\dagger$	$\alpha_1{}^\S$	$\alpha_2{}^\S$	τ_1 (ns)¶	τ_2 (ns)¶	$f_1{}^\|$	$f_2{}^\|$	$\langle\tau\rangle$ (ns)**	$\bar{\tau}$ (ns)††
1.0	2	0.26 (0.25–0.27)§§	0.74 (0.73–0.75)	2.25 (2.22–2.27)	4.38 (4.37–4.39)	15.4	84.6	4.05	3.82
2.1	1	0.18 (0.17–0.19)	0.82 (0.81–0.83)	2.09 (2.04–2.14)	4.26 (4.25–4.27)	9.9	90.1	4.04	3.86
5.8	1	0.20 (0.19–0.22)	0.80 (0.78–0.81)	2.24 (2.16–2.35)	4.20 (4.18–4.23)	12.0	88.0	3.97	3.81
16.3	1	0.17 (0.16–0.19)	0.83 (0.81–0.85)	2.06 (1.95–2.21)	4.16 (4.14–4.19)	9.4	90.6	3.96	3.80
33.9	1	0.22 (0.21–0.24)	0.78 (0.76–0.79)	2.13 (2.06–2.20)	4.02 (3.99–4.04)	13.2	86.8	3.77	3.59
68.9	1	0.21 (0.20–0.22)	0.79 (0.78–0.80)	2.35 (2.32–2.38)	4.10 (4.09–4.11)	13.4	86.7	3.87	3.73

| η^* | ϕ_e (ns)¶¶ | $\phi_e/\langle\tau\rangle^{\|\|\|}$ | Without constraint | | | | With constraint | | | | |
			ϕ (ns)***	$\beta_1{}^{\dagger\dagger\dagger}$	$\beta_2{}^{\S\S\S}$	$\chi^2{}^{\P\P\P}$	ϕ (ns)***	$\beta_1{}^{\dagger\dagger\dagger}$	$\beta_2{}^{\S\S\S}$	$\chi^2_C{}^{\P\P\P}$	$r_{ss}{}^{\|\|\|\|}$
1.0	5.9	1.5	6.2 (6.0–6.4)	0.234 (0.213–0.254)	0.200 (0.189–0.212)	1.096	5.9 (5.8–6.0)	0.202 (0.183–0.217)	0.209 (0.203–0.214)	1.097	0.124
2.1	12.4	3.1	14.7 (13.9–15.7)	0.201 (0.180–0.227)	0.217 (0.211–0.222)	1.068	12.3 (12.1–12.5)	0.138 (0.131–0.146)	0.208 (0.207–0.209)	1.072	0.151
5.8	34.2	8.6	21.5 (16.1–27.4)	0.128 (0.079–0.183)	0.132 (0.117–0.149)	1.058	38.8 (37.2–40.7)	0.227 (0.219–0.237)	0.189 (0.187–0.191)	1.061	0.176
16.3	96	24.2	122 (94–156)	0.347 (0.311–0.390)	0.276 (0.250–0.304)	1.113	91 (73–107)	0.276 (0.247–0.303)	0.195 (0.191–0.199)	1.114	0.194
33.9	200	53	96 (58–152)	0.081 (0.052–0.118)	0.100 (0.084–0.120)	1.138	192 (163–231)	0.182 (0.173–0.194)	0.203 (0.201–0.204)	1.139	0.196
68.9	407	105	66 (56–75)	0.130 (0.089–0.163)	0.185 (0.177–0.196)	1.092	81 (76–87)	0.166 (0.156–0.177)	0.215 (0.213–0.217)	1.090	0.199

*Viscosity (in cP).

†Number of datasets. If $n > 1$, the reported results are averages except for χ^2.

§Recovered amplitudes normalized to a sum of one.

¶Recovered fluorescence intensity decay lifetimes.

$^\|$Percent contribution to total emission: $f_i = 100\alpha_i\tau_i/\Sigma\alpha_i\tau_i$.

**Intensity average lifetime: $\langle\tau\rangle = \Sigma\alpha_i\tau_i^2/\Sigma\alpha_i\tau_i$.

††Number average lifetime: $\bar{\tau} = \Sigma\alpha_i\tau_i/\Sigma\alpha_i$.

§§95% confidence interval.

¶¶The expected ϕ based on the recovered ϕ at 1 cP and the linear relationship between ϕ and η (Stokes-Einstein equation; see text).

$^{\|\|\|}$Ratio of expected correlation time to the intensity average lifetime.

***Recovered rotational correlation time.

†††Limiting anisotropy recovered for the species having a lifetime of τ_1.

§§§Limiting anisotropy recovered for the species having a lifetime of τ_2.

¶¶¶The reduced, weighted sum of residuals. If $n > 1$, the reported value is for one representative dataset.

$^{\|\|\|\|}$The measured steady-state anisotropy used as the constraint.

components each appear to be viscosity-independent, with the short lifetime (τ_1) component contributing only a small (10–15%) fraction of the total emission intensity (Table 3). We also have determined that the intensity decay parameters are independent of emission wavelength (not shown). As was found with the rat parvalbumin datasets, analyses with and without the r_{ss} constraint do not yield different intensity decay parameters. In addition, the excellent quality of fitting was the same with or without the constraint; this can be noted by the χ^2 terms in Table 3. Although the relative amplitude terms do not exhibit a distinct change with increasing glycerol (Table 3), the longer cod parvalbumin lifetime (τ_2) shows a small but significant decrease (except for the 69 cP dataset). This trend, as was noted for the rat F102W

parvalbumin results, is also reflected in the number and intensity lifetime averages.

The anisotropy decay of the cod protein closely resembles that observed for the rat protein. Only a single correlation time is required (Table 3). Because the two proteins are essentially the same size, the value recovered at 1 cP is the same as that for the mutant rat parvalbumin. The need for only a single correlation time implies that the reporting Trp residues in the hydrophobic core of both parvalbumins appear to undergo no local motions leading to depolarization. The two proteins also exhibit similar viscosity-dependent trends in recovered parameters. Without the r_{ss} constraint, analyses of the cod parvalbumin datasets failed to recover the expected correlation times for all viscosities

above 1 cP. Upon application of the constraint, the expected correlation time was recovered for all datasets up through 34 cP (Table 3). If we assume that the two lifetimes observed for the cod protein are associated with different ground-state forms of the Trp residue, each lifetime should have a β term associated with it that represents the r_0 of the fluorophore. Consequently, as is true for the rat parvalbumin data, the β values associated with each of the cod protein lifetimes should be near 0.2 and viscosity independent. For analyses without the r_{ss} constraint, the range of recovered β_1 values is significantly larger than that for β_2. Because both β terms did not become smaller with increasing viscosity, as was observed for the rat protein datasets analyzed without the constraint, both return an average value near 0.2 over the set of viscosities. With the constraint applied, both β terms have a smaller range of values over all viscosities, although the range for β_1 is still wider than that for β_2 (Table 3). Again, the average of each β term over the viscosities is near 0.2. The larger range of values for β_1 probably reflects the small contribution of the first exponential component (τ_1) to the total emission and, consequently, larger uncertainty in the associated anisotropy parameter.

To complete the evaluation of the cod parvalbumin results, we generated uncertainty plots for the single correlation time and both β terms. As shown in Fig. 5, the use of the constraint greatly improves the precision for all three parameters, particularly both β terms. With the r_{ss} constraint, the uncertainty in β_2 is below 5% (Fig. 5 C) and the uncertainty in β_1 is near 10% (Fig. 5 B), even though this is associated with the form contributing only 10–15% of the fluorescence. It is interesting that without the constraint, the uncertainty in β_1 for the 16 cP sample is essentially the same as with the constraint. It should be noted, however, that the value recovered for β_1 at 16 cP is much less accurate without the constraint (Table 3), and that an analysis without the constraint took 1000–2000 iterations (depending on initial guesses) to converge whereas with the constraint it only took 10–20 iterations (guess independent). Except for the 69 cP sample, the uncertainty in the recovered correlation time tends to increase with viscosity as is observed with the rat parvalbumin (Fig. 4 A).

DISCUSSION

Interpretation of time-resolved fluorescence anisotropy decay results is often limited by imprecise determination of cross-correlated parameters. This limitation is compounded when there are multiple intensity decay lifetimes and multiple anisotropy decay correlation times, which also raises the issue of unknown associations between lifetimes and correlation times. Another limitation is that the fluorescence lifetimes of commonly used probes are short compared to the rotational correlation times of many biomolecules and their assemblies. Our recently introduced analysis procedures are initial steps toward addressing these
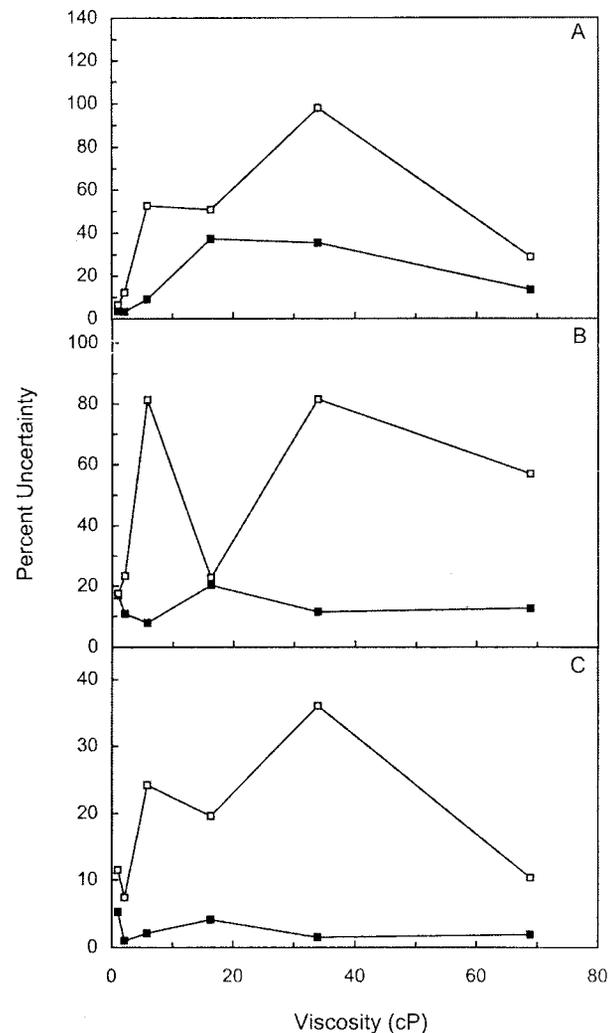
FIGURE 5 Percent uncertainties in iterated parameter values as a function of viscosity for cod parvalbumin. (A) Uncertainties in recovered correlation times. (B) Uncertainties in recovered β_1 terms. (C) Uncertainties in recovered β_2 terms. Filled/open markers represent analyses with/without the r_{ss} constraint. Lines connect related data points and do not represent any model.

limitations by increasing the dynamic and conformational information that can be resolved from fluorescence anisotropy decay data (Bialik et al., 1998; Rachofsky et al., 1999).

Our previous simulation studies showed that application of the steady-state anisotropy as a constraint during data analysis increased the accuracy of recovered parameters as well as demonstrated in principle that rotational correlation times much longer than the lifetime could be resolved (Rachofsky et al., 1999). In these simulation studies, the precision of recovered parameters also was qualitatively improved on application of the r_{ss} constraint. To test these observations from simulations experimentally, we have examined the fluorescence anisotropy decays of single Trp residues in two parvalbumins as a function of viscosity.

Different viscosities were employed to increase the expected ϕ/τ ratio by close to two orders of magnitude, and different excitation wavelengths were used to vary the limiting anisotropy. The rat F102W parvalbumin represents the simplest possible experimental model system. Based on the structure of rat parvalbumin (McPhalen et al., 1994), the shape of the protein is essentially spherical, which will yield a single rotational correlation time. In addition, the Trp residue buried in the hydrophobic core of the protein exhibits no local depolarizing motions and minimal glycerol solvent effects. Finally, the fluorescence intensity decay of the single Trp residue is a single exponential. The calcium-bound form of the cod parvalbumin shares these properties of the rat parvalbumin, except that a sum of two exponentials is needed to describe its intensity decay. Consequently, the cod parvalbumin is a more complicated kinetic system, but one that is more general and thus provides an excellent extension for testing the analysis procedure.

Comparison with simulation studies

The results of our experiments show good agreement with most of the predictions from the previously published simulations (Rachofsky et al., 1999). As expected, application of the constraint did not alter fitting statistics (χ^2) or graphical representations of the quality of fitting (residuals and autocorrelation of residuals), but did enhance the accuracy and precision of recovered parameters. Comparison of the experimental and simulation results was facilitated by the fact that our recovered r_0 values (0.2 and 0.05 at 295- and 290-nm excitation, respectively) are similar to r_0 values employed in the simulations (0.3, 0.15, and 0.05). A key observation from the simulations was that the r_{ss} constraint should enhance recovery of larger ϕ/τ ratios. In agreement, accurate parameter recovery (both ϕ and β) could not be obtained by unconstrained analysis for $\phi/\tau \geq 3$ from experimental datasets having the larger r_0 (295-nm excitation). With application of the r_{ss} constraint, however, correlation times were accurately recovered from rat protein datasets obtained with 295-nm excitation for a ϕ/τ ratio up to 25 (Table 1 and Fig. 2). Moreover, the correlation time for a sample with a ϕ/τ ratio near 50 (Table 3) was accurately determined for the cod protein data. This is in very good agreement with the simulations, where accurate parameters were recovered for maximum ϕ/τ ratios of 30 and 100 for r_0 values of 0.15 and 0.3, respectively (Rachofsky et al., 1999). Another prediction of the simulations was that smaller r_0 values should hinder accurate parameter recovery. In fact, for those mutant rat parvalbumin datasets excited at 290 nm where the r_0 was small (0.05), physically relevant parameters could not be recovered for samples at the higher viscosities without the use of the r_{ss} constraint. However, on application of the r_{ss} constraint, the expected region for accurate recovery extended to a ϕ/τ ratio near 10 (Table 2, Fig. 3), in agreement with that estimated by simulations (Rachofsky

et al., 1999). The experimental results for both the rat F102W and cod parvalbumins confirm the simulation prediction that the recoverable (useful) range of ϕ/τ ratio can be extended by at least an order of magnitude through use of the r_{ss} constraint during data analysis.

Parameter precision

Recovered parameters from constrained analyses should be not only more accurate but also more precise than those from unconstrained analyses (Rachofsky et al., 1999). The improvement in precision arising from a constrained analysis can be visualized by considering a χ^2 surface. Without the constraint, the χ^2 minimum corresponding to accurate parameter values can be obscured from the searching procedure by the flatness of the surface. With a constraint, the gradient around the minimum value steepens considerably because the iterated parameter values not only must fit the data, but also must generate the measured steady-state anisotropy. The percent uncertainties shown in Figs. 4 and 5 demonstrate that the r_{ss} constraint improves the precision of the parameters recovered from experimental data. Consequently, in accordance with the initial suggestion (Rachofsky et al., 1999), the present results demonstrate that the r_{ss} constraint facilitates more accurate and more precise recovery of anisotropy parameters. Importantly, application of the constraint also has these effects on recovered parameters for the cod parvalbumin, a more complex kinetic system in which one of the exponential components contributed only 10–15% of the total fluorescence.

Constraint function limitation

The dependence of recovered anisotropy parameter precision and accuracy on viscosity differs between β and ϕ. Without the constraint, the ϕ terms were recovered accurately at lower viscosities, and deviated systematically from expected values with increasing viscosity. The effect of the constraint was to increase the range of viscosities at which ϕ values could be accurately recovered, and to increase the precision of the correlation time at higher viscosities. In contrast, without the r_{ss} constraint, the β terms deviated either systematically (rat protein) or randomly (cod protein) from the expected value at low viscosities, even those at which correlation times were recovered accurately. With the constraint, however, the recovered β terms were always close to the expected value, even when the correlation time was not accurately recovered. These differences in parameter tendency on application of the constraint are directly related to the differing dependence of the calculated steady-state anisotropy, r_{calc}, on β and ϕ. As the correlation time increases, the τ/ϕ term in the denominator of Eq. 8 loses its contribution to r_{calc}. Consequently, even constrained analyses become insensitive to the value of ϕ when it is much greater than τ. However, the contribution of r_0 to r_{calc} is

essentially independent of viscosity. Therefore, in any constrained analysis, the β term will be iterated to a value that permits r_{calc} to equal the measured r_{ss}. Because the measured r_{ss} approaches the r_0 of the Trp residue as viscosity increases, the recovered β term for this system with a single correlation time is the expected r_0 value. This numerical argument explains why this constraint function is unable to help recover the larger correlation times for the parvalbumin samples in the highest viscosity solutions. Consequently, caution needs to be exercised not only in selecting the constraint function, but also in assessing how the calculated component can maximize or minimize the contribution of one or more iterated parameters.

The measured steady-state anisotropy

The initial simulation results indicated that an accurate steady-state anisotropy value is essential for it to be effective as a constraint (Rachofsky et al., 1999). In those simulation studies, errors in the measured r_{ss} resulted in inaccurate recovery of anisotropy decay parameters from constrained analyses. Similar effects have been observed for several rat F102W parvalbumin anisotropy decay datasets (not shown). This need for an accurate steady-state anisotropy value can be understood because a change in the r_{ss} constraint will require a corresponding change in r_{calc} (as shown in Eqs. 7 and 8), which will result in a change in the recovered values of both β and ϕ. Consequently, it is necessary to obtain the steady-state anisotropy value under optical conditions as close as possible to those employed to the time-resolved measurement. Ideally, as was done in these studies, both the steady-state and time-resolved measurements should be carried out on the same instrument.

Comparison to other analysis procedures

Other studies have previously employed the steady-state anisotropy to help direct the analyses of time-resolved fluorescence anisotropy decay data (Blumberg et al., 1974; Vanderkooi et al., 1974; Dale, 1983). As discussed in our previous study (Rachofsky et al., 1999), none of these methods offer any advantage over the current method. Furthermore, these methods differ from the current algorithm in that they employ the steady-state anisotropy to help scale the vertical and horizontal decay curves for data analysis, and do not directly affect iterated parameters during data analyses.

There are other approaches that can be used to help recover parameters when there is failure to resolve parameter values and/or mechanisms. For example, one or more parameters, such as β and ϕ terms, may be fixed to a known value and the remaining parameters iterated. However, it is not always easy to estimate or independently measure those parameters accurately. Importantly, the constrained analysis

approach used in the present studies does not fix parameters to specific values. Instead, constrained parameter values are allowed to vary during the minimization of χ^2 with the contribution of each parameter to the "goodness of fit" weighted by its respective uncertainty (Rachofsky et al., 1999).

Global analysis is another approach to resolve a variety of kinetic models and parameters with similar magnitudes (Knutson et al., 1983; Beechem et al., 1983). In a global analysis, multiple datasets taken as function of an independent variable are analyzed simultaneously, making one or more iterated parameters common to all datasets based on a kinetic model. We therefore compared the effectiveness of the r_{ss} constraint versus global analysis to recover anisotropy decay parameters. Because for our single correlation time system the β term (r_0) relates to the angle between the absorption and emission transition dipole moments, it is not expected to be dependent on viscosity, and therefore can be used as a common parameter between datasets. Global analyses were performed, with no constraint applied, on datasets grouped by protein and excitation wavelength. All results were compared to the expected values used in the evaluation of the individual r_{ss} constrained analyses. As judged by the recovered correlation times and an overall recovery parameter introduced for the simulation studies (Rachofsky et al., 1999), the two global analyses for rat protein datasets and the global analysis for the cod parvalbumin datasets consistently recovered parameters better than the unconstrained analyses of single curves. The recovered values for the common β terms were 0.05 and 0.2 for the datasets excited at 290 and 295 nm, respectively, in agreement with the values recovered at all viscosities by r_{ss} constrained analysis. Similar correspondences were obtained from a global analysis of the cod protein datasets. Further, the steady-state anisotropies, which were calculated from the parameters recovered from global analyses, corresponded closely to the measured values for those viscosities. It is noteworthy that the global analyses began to fail recovering parameters at the same viscosities, that is, the same ϕ/τ ratios, as the constrained analyses. For data obtained with 295-nm excitation, the overall recovery of parameters for both proteins from global analysis was similar to that from constrained analyses. However, the overall parameter recovery from the global analysis of the rat parvalbumin datasets obtained with 290-nm excitation was intermediate between those obtained from the unconstrained and constrained analyses. In summary, the analysis of a *single* dataset using the r_{ss} constraint consistently recovered parameters at least as well as the global analysis of several datasets collected as a function of viscosity, and better than global analysis for systems with a small r_0. Consequently, a constrained analysis of a single dataset can yield important information, especially when a global analysis is not possible because an independent variable does not exist for the system under study.

Effect of glycerol on fluorescence lifetime

The single intensity decay lifetime for the lone Trp residue in the rat parvalbumin and the longer of the two lifetimes for the single Trp residue in cod parvalbumin decrease slightly with increasing glycerol concentration (Tables 1–3). It was observed previously that the apo state of the rat F102W parvalbumin has a slightly shorter lifetime ($\sim$3.8 ns) than its Ca^{2+}-bound state (Pauls et al., 1993). Consequently, an initial explanation for the lifetime decreases could be a glycerol-dependent equilibrium between the calcium-bound and apo forms. This possibility, however, can be dismissed because both parvalbumins examined here bind calcium tightly, with nanomolar dissociation constants (Pauls et al., 1993; Permiakov et al., 1987). Because these experiments were performed in the presence of 5 mM calcium, for significant loss of calcium binding to occur, the affinity for parvalbumin would have to decrease by many orders of magnitude upon addition of glycerol. Moreover, no perturbation of the fluorescence was observed upon addition of glycerol. Consequently, it can be reasoned that emission is always observed from the Ca^{2+}-bound state. At present, we have no explanation for the small decrease in fluorescence lifetime(s) for the buried Trp residue in either parvalbumin that accompanies the increase in glycerol concentration.

Future studies and conclusions

Our studies have demonstrated that application of the steady-state anisotropy as a constraint during the analysis of time-resolved fluorescence anisotropy decay data can facilitate more accurate, precise determination of longer correlation times. Parameter recovery may be improved further by combining the r_{ss} constraint procedure with other analytical methods or physical techniques. Additional ways of limiting parameter values and/or possible kinetic models will be particularly useful with those systems requiring multiple lifetimes and correlation times. For example, we will try to apply the r_{ss} constraint with our newly developed method for assigning lifetime-correlation time associations (Bialik et al., 1998). We will also examine the use of more than one constraint during an analysis. The right side of Eq. 6 can actually be stated as $\chi^2 + \Sigma\kappa_p g_p$, provided that other independent measurements could be made of quantities that can also be calculated from iterated parameters. For example, in a multiple lifetime, multiple correlation time system, the sum of the β_{ij} terms over j must equal the r_0 for species i. Consequently, both r_0 and r_{ss} constraints could be applied together to help limit the range of values for anisotropy decay parameters. We also will try to include information from other techniques. For example, size and shape parameters obtained from hydrodynamic studies, such as with the analytical ultracentrifuge, could provide values for fixing certain correlation times or limiting their values during an analysis. Finally, we have begun an assessment of combining the r_{ss} constraint with the global analysis of multiple datasets.

Despite the need for further studies defining the capability of constrained analysis of fluorescence anisotropy decay, it is evident from the current results that this technique may now be applied more broadly as a tool to elucidate the dynamics of biological systems. As a result of these studies, it is now possible to extract much more information than ever before about local, segmental, and overall dynamics and hydrodynamics of proteins and other biomolecules from time-resolved anisotropy data.

REFERENCES

Badea, M., and L. Brand. 1979. Time-resolved fluorescence measurements. *Methods Enzymol.* 61:378–425.

Beechem, J. M., J. R. Knutson, J. B. A. Ross, B. W. Turner, and L. Brand. 1983. Global resolution of heterogeneous decay by phase/modulation fluorometry: mixtures and proteins. *Biochemistry.* 22:6054–6058.

Bevington, P. R. 1969. Data Reduction and Error Analysis for the Physical Sciences. McGraw-Hill, New York.

Bialik, C. N., B. Wolf, E. L. Rachofsky, J. B. A. Ross, and W. R. Laws. 1998. Dynamics of biomolecules: assignment of local motions by fluorescence anisotropy decay. *Biophys. J.* 75:2564–2573.

Blumberg, W. E., R. E. Dale, J. Eisinger, and D. Zuckerman. 1974. Energy transfer in the tRNA[Phe] (yeast). The solution structure of transfer RNA. *Biopolymers.* 13:1607–1620.

Closset, J. I. 1976. Parvalbumins of white muscle of gadidae. 1. Extraction and purification of the parvalbumins of the whiting (*Gadus merlangus L.*), of the coalfish (*G. virens L.*), and of the haddock (*G. aeglefinus L.*). *Comp. Biochem. Physiol. B.* 55:531–535.

Cross, A. J., and G. R. Fleming. 1984. Analysis of time-resolved fluorescence anisotropy decays. *Biophys. J.* 46:45–56.

Dale, R. E. 1983. Membrane structure and dynamics by fluorescence probe depolarization kinetics. *In* Time-Resolved Fluorescence Spectroscopy in Biochemistry and Biology, R.B. Cundall and R.E. Dale, editors. Plenum Press, New York. 555–604.

Declerc, G. P., C. Evrard, V. Lamzin, and J. Parello. 1999. Crystal structure of the EF-hand parvalbumin at atomic resolution (0.91 Å) and at low temperature (100 K). Evidence for conformational multistates within the hydrophobic core. *Protein Sci.* 8:2194–2204.

Eftink, M. R., and Z. Wasylewski. 1989. Fluorescence lifetime and solute quenching studies with the single tryptophan containing protein parvalbumin from codfish. *Biochemistry.* 28:382–391.

Eftink, M. R., L. A. Selvidge, P. R. Callis, and A. A. Rehms. 1990. Photophysics of indole derivatives: experimental resolution of ^1L_a and ^1L_b transitions and comparison with theory. *J. Phys. Chem.* 94:3469–3479.

Feinstein, E., E. Rusinova, G. Deikus, E. L. Rachofsky, J. B. A. Ross, and W. R. Laws. 2001. Local and rotational dynamics of calcium-binding proteins: new analysis methods for time-resolved fluorescence anisotropy. *Biophys. J.* 80:361a. (Abstr.)

Grinvald, A., and I. Z. Steinberg. 1974. On the analysis of fluorescence decay kinetics by the method of least squares. *Anal. Biochem.* 59:583–598.

Haydock, C., J. C. Sharp, and F. G. Prendergast. 1990. Tryptophan-47 rotational isomerization in variant-3 scorpion neurotoxin. A combination thermodynamic perturbation and umbrella sampling study. *Biophys. J.* 57:1269–1279.

Hutnik, C. M. L., J. P. MacManus, and A. G. Szabo. 1990. A calcium specific conformational response of parvalbumin. *Biochemistry.* 29:7318–7328.

Kawasaki, H., and R. H. Kretsinger. 1994. Calcium-binding proteins. 1: EF-hands. *Protein Profile.* 1:343–517.

Kim, S. J., F. N. Chowdhury, W. Styjewski, E. S. Younathan, P. S. Russo, and M. D. Barkley. 1993. Time-resolved fluorescence of the single tryptophan of bacillus stearothermophilus phosphofructokinase. *Biophys. J.* 65:215–226.

Knutson, J. R., J. M. Beechem, and L. Brand. 1983. Simultaneous analysis of multiple fluorescence decay curves: a global approach. *Chem. Phys. Lett.* 102:501–507.

Kretsinger, R. H. 1980. Structure and evolution of calcium-modulated proteins. *CRC Crit. Rev. Biochem.* 8:119–174.

Kretsinger, R. H., and C. E. Nockolds. 1973. Carp muscle calcium binding protein. II. Structural determination and general description. *J. Biol. Chem.* 248:3313–3326.

Laberge, M., W. W. Wright, K. Sudhakar, P. A. Liebman, and J. M. Vanderkooi. 1997. Conformational effects on calcium release from parvalbumin: comparison of computational simulations with spectroscopic investigations. *Biochemistry.* 36:5363–5371.

Lakowicz, J. R. 1999. Principles of Fluorescence Spectroscopy, 2nd ed. Kluwer Academic/Plenum Publishing, New York.

McPhalen, C. A., A. R. Sielecki, B. D. Santarsiero, and M. N. James. 1994. Refined structure of rat parvalbumin, a mammalian alpha-lineage parvalbumin, at 2.0 Å resolution. *J. Mol. Biol.* 235:718–732.

Nakayama, S., and R. H. Kretsinger. 1994. Evolution of the EF-hand family proteins. *Annu. Rev. Biophys. Biomol. Struct.* 23:473–507.

Pauls, T. L., I. Durussel, J. A. Cox, I. D. Clark, A. G. Szabo, S. M. Gagne, B. D. Sykes, and M. W. Berchtold. 1993. Metal binding properties of recombinant rat parvalbumin wild-type and F102W mutant. *J. Biol. Chem.* 268:20897–20903.

Permiakov, E. A., A. V. Ostroyskii, L. P. Kalinichenko, and G. I. Deikus. 1987. Kinetics of dissociation of parvalbumin complexes with calcium and magnesium ions. *Mol. Biol.* 21:1017–1022.

Petrich, J. W., M. C. Chang, D. B. McDonald, and G. R. Fleming. 1983. On the origin of nonexponential fluorescence decay in tryptophan and its derivatives. *J. Am. Chem. Soc.* 105:3824–3832.

Rachofsky, E. L., and W. R. Laws. 2000. Kinetic models and data analysis methods for fluorescence anisotropy decay. *Methods Enzymol.* 321:216–238.

Rachofsky, E. L., B. Wolf, C. N. Bialik, J. B. A. Ross, and W. R. Laws. 1999. A general method for constrained analysis of fluorescence anisotropy decay: application of the steady-state anisotropy. *J. Fluorescence.* 9:379–390.

Ross, J. B. A., H. R. Wyssbrod, R. A. Porter, G. P. Schwartz, C. A. Michaels, and W. R. Laws. 1992. Correlation of tryptophan fluorescence intensity decay parameters with ^{1}H NMR-determined rotamer conformations: [tryptophan]^{2}oxytocin. *Biochemistry.* 31:1585–1594.

Sheely, M. L. 1932. Glycerol viscosity tables. *Ind. Eng. Chem.* 24:1060–1064.

Straume, M., S. G. Frasier-Cadoret, and M. L. Johnson. 1991. Least-squares analysis of fluorescence data. *In* Topics in Fluorescence Spectroscopy, Vol 2. J.R. Lakowicz, editor. Plenum Press, New York. 177–240.

Szabo, A. G., and D. M. Rayner. 1980. Fluorescence decay of tryptophan conformers in aqueous solution. *J. Am. Chem. Soc.* 102:554–563.

Vanderkooi, J., S. Fischkoff, B. Chance, and R. A. Cooper. 1974. Fluorescent probe analysis of the lipid architecture of natural and experimental cholesterol-rich membranes. *Biochemistry.* 13:1589–1595.

Wahl, Ph. 1979. Analysis of fluorescence anisotropy decays by a least squares method. *Biophys. Chem.* 10:91–104.

Waxman, E., W. R. Laws, T. M. Laue, Y. Nemerson, and J. B. A. Ross. 1993. Human factor VIIa and its complex with soluble tissue factor: evaluation of asymmetry and conformational dynamics by ultracentrifugation and fluorescence anisotropy decay methods. *Biochemistry.* 32:3005–3012.

Wetlaufer, D. B. 1962. Ultraviolet spectra of proteins and amino acids. *Adv. Prot. Chem.* 17:303–390.

Willis, K. J., and A. G. Szabo. 1992. Conformation of parathyroid hormone: time-resolved fluorescence studies. *Biochemistry.* 31:8924–8931.